

# Bimetallic Catalysts for the Efficient Growth of SWNTs on Surfaces

Xuan Wang, Wenbo Yue, Maoshuai He, Manhong Liu, Jin Zhang,\* and Zhongfan Liu\*

Center for Nanoscale Science and Technology (CNST), College of Chemistry and Molecular Engineering, Peking University, Beijing 100871, P. R. China

Received October 26, 2003

Bimetallic catalysts such as Fe/Ru and Fe/Pt in the size range of 0.5–3 nm are currently being considered for the efficient growth of single-walled carbon nanotubes (SWNTs) on flat surfaces. It has been shown possible, by using chemical reduction under microwave irradiation and poly(*N*-vinyl-2-pyrrolidone) (PVP) as a protective agent, to produce uniform Fe/Ru and Fe/Pt bimetallic nanoparticles. Energy-dispersive X-ray analysis (EDAX) confirmed the presence of Fe and Ru or Fe and Pt, and high-resolution transmission electron microscopy (HRTEM) showed that they were highly crystalline. The nanoparticles were subsequently used as catalysts for the surface growth of SWNTs by chemical vapor deposition (CVD). When compared with single-component catalysts such as Fe, Ru, and Pt of similar size, bimetallic catalysts Fe/Ru and Fe/Pt produced at least 200% more SWNTs, as measured by atomic force microscopy (AFM). Possible reasons for the high efficiency of bimetallic catalysts are discussed in this study.

## Introduction

There has been significant progress in both the production and application of carbon nanotubes since their discovery in 1991.<sup>1</sup> The unique properties of single-walled carbon nanotubes (SWNTs) have made them ideal candidates for components in nanoelectronics devices, such as quantum wires,<sup>2,3</sup> flat-panel field emission displays,<sup>4</sup> and field-effect transistors.<sup>5</sup> Most of these devices have employed SWNTs produced by catalyzed bulk growth and by depositing them from solvents onto surfaces. In the catalyzed bulk synthesis of SWNTs, catalysts such as Fe, Co, Ni, Cu, Ru,<sup>17–19</sup> and bimetallic

systems such as Fe/Mo,<sup>20</sup> Fe/Ru,<sup>20</sup> and Co/Pt<sup>21</sup> have been investigated. However, catalytic bulk growth of SWNTs involves purification and dispersion steps which may result in defects on the SWNTs surfaces. SWNTs produced in this way are also very difficult to orient.

Catalytic surface growth of SWNTs, on the other hand, can produce surface-oriented defect-free nanotubes.<sup>6–8</sup> Initial studies have indicated that a key factor in the surface growth via chemical vapor deposition (CVD) is the preparation of preformed catalysts.<sup>9–16</sup> An effective approach has been to use discrete catalytic nanoparticles on flat substrates,<sup>10–16</sup> such as dendrimer carriers<sup>11</sup> and metal-containing molecular nanoclusters.<sup>14</sup> This approach has also permitted effective control of the diameter and structure of SWNTs.<sup>16</sup>

The preparation of discrete nanoparticles as catalysts for the surface growth of SWNTs is still in its infancy. Until now, the catalytic surface growth of SWNTs has been limited to the use of 1–13 nm Fe<sup>8,10–12,16</sup> and Fe/Mo<sup>7,13–15</sup> nanoparticles. Therefore, there still remains significant room for the rational design and fabrication of new catalysts in the field of SWNTs surface growth.

Because of their unique chemical and physical properties, the production of nanoparticle catalysts has been widely explored. Recently, chemical reduction associated with microwave irradiation has been adopted to prepare noble metal nanoparticles<sup>22–24</sup> such as Pt, Rh, Ir, Pd,

\* To whom correspondence should be addressed. Phone/Fax: 86-10-6275-7157. E-mail: jzhang@chem.pku.edu.cn.

- (1) Iijima, S. *Nature* **1991**, *354*, 56.
- (2) Appenzeller, J.; Martel, R.; Avouris, P. et al. *Appl. Phys. Lett.* **2001**, *78*, 3313.
- (3) Collins, P. G.; Zettl, A.; Bando, H. et al. *Science* **1997**, *278*, 100.
- (4) Rinzler, A. G.; Hafner, J. H.; Nikolaev, P.; Lou, L.; Kim, S. G. *Science* **1995**, *269*, 1550.
- (5) Tans, S. J.; Devoret, M. H.; Dai, H. J. et al. *Nature* **1997**, *38*, 474.
- (6) Lee, K. H.; Cho, J. M.; Sigmund, W. et al. *Appl. Phys. Lett.* **2003**, *82*, 448.
- (7) Huang, S. M.; Cai, X. Y.; Liu, J. et al. *J. Am. Chem. Soc.* **2003**, *125*, 5636.
- (8) Joselevich, E.; Lieber, C. M. et al. *Nano Lett.* **2002**, *2*, 1137.
- (9) Jing K.; Soh, H. T.; Cassell, A. M.; Quate, C. F.; Dai, H. J. *Nature* **1998**, *395*, 878.
- (10) Li, Y. M.; Kim, W.; Zhang, Y. G.; Dai, H. J. et al. *J. Phys. Chem. B.* **2001**, *105*, 11424.
- (11) Choi, H. C.; Kim, W.; Wang, D. V.; Dai, H. J. *J. Phys. Chem. B.* **2002**, *106*, 12361.
- (12) Choi, H. C.; Kundaria, S.; Wang, D. W.; Dai, H. J. et al. *Nano Lett.* **2003**, *3*, 157.
- (13) Li, Y.; Liu, J. et al. *Chem. Mater.* **2001**, *13*, 1008.
- (14) An, L.; Owens, J. M.; McNeil, L. E.; Liu, J. *J. Am. Chem. Soc.* **2002**, *124*, 13688.
- (15) Zheng, B.; Lu, C. G.; Gu, G.; Liu, J. et al. *Nano Lett.* **2002**, *2*, 895.
- (16) Cheung, C. L.; Kurtz, A.; Park, H.; Lieber, C. M. *J. Phys. Chem. B.* **2002**, *106*, 2429.

(17) Mabudafhasi, M. L.; Bodkin, R.; Nicolaides, C. P.; Coville, N. *J. Carbon* **2002**, *40*, 2737.

(18) Randall, L.; Vander, W.; Ticich, T. M.; Curtis, V. E. et al. *Carbon* **2001**, *39*, 2277.

(19) Luo, G. H.; Li, Z. F.; Wei, F.; Deng, X. Y.; Yong, J. et al. *Physica B* **2002**, *323*, 314.

(20) Cassell, A. M.; Kong, J.; Dai, H. J. et al. *J. Phys. Chem. B.* **1999**, *103*, 6484.

(21) Brotons, V.; Coq, B.; Planeix, J. M. *J. Mol. Catal. A: Chem.* **1997**, *116*, 397.

and Ru. Compared with conventional heating, microwave irradiation provides a rapid and homogeneous heating environment for the nucleation process and leads to the formation of uniform nanoparticles.<sup>22–24</sup> In the present study, we have modified a method of producing noble metal nanoparticles through chemical reduction under microwave irradiation<sup>22–24</sup> to obtain bimetallic nanoparticles such as Fe/Ru and Fe/Pt. These uniform, polymer-stabilized nanoparticles, 0.5–3 nm diameter, were subsequently used as catalysts for the growth of SWNTs on silica surfaces. Compared with single metal Fe, Ru, and Pt nanoparticles of similar size, the use of bimetallic catalysts Fe/Pt and Fe/Ru improved the production of SWNTs by at least 200%. Thus, the present work offers a simple way of producing Fe/Ru and Fe/Pt alloy nanoparticles as well as the efficient and reproducible surface growth of SWNTs.

### Experimental Section

**Materials.** Poly(*N*-vinyl-2-pyrrolidone) (PVP, av. MW 40 000) was obtained from Fluka. Other analytical reagents including  $\text{RuCl}_3 \cdot 3\text{H}_2\text{O}$ ,  $\text{FeCl}_3$ , and  $\text{H}_2\text{PtCl}_6 \cdot 6\text{H}_2\text{O}$  were purchased from Beijing Chemical Corporation and used as received.

**Synthesis of Single-Component Nanoparticles: Pt, Ru,<sup>22–24</sup> and Fe.**  $\text{H}_2\text{PtCl}_6 \cdot 6\text{H}_2\text{O}$  ( $5 \times 10^{-6}$  mol; 0.0026 g) and PVP ( $2.5 \times 10^{-4}$  mol; 0.0287 g) were dissolved in 4.8 mL of glycol. The mixture was stirred for 5 min, and then 0.2 mL of a glycol solution of ammonia (0.2 M) was added dropwise with vigorous stirring for another 5 min. The beaker with solution was then put into the center of a household microwave oven (2450 MHz, WP 750). After 30 s microwave irradiation, the orange solution changed to black due to the formation of PVP-stabilized Pt colloid. The influence of amounts of PVP and  $\text{H}_2\text{PtCl}_6 \cdot 6\text{H}_2\text{O}$  on the size of nanoparticles was discussed previously.<sup>22–24</sup> In our study, we fixed the initial molar ratio, PVP/ $\text{H}_2\text{PtCl}_6 \cdot 6\text{H}_2\text{O}$  to 50 to control the average size of nanoparticles at 1.5–2 nm.<sup>24</sup> Likewise, substituting 0.0013 g of  $\text{RuCl}_3 \cdot 3\text{H}_2\text{O}$  ( $5 \times 10^{-6}$  mol) or 0.0008 g of  $\text{FeCl}_3$  ( $5 \times 10^{-6}$  mol) for 0.0026 g of  $\text{H}_2\text{PtCl}_6 \cdot 6\text{H}_2\text{O}$ , we obtained ruthenium or iron nanoparticles.

**Synthesis of Bimetallic Nanoparticles: Fe/Ru and Fe/Pt.**  $\text{RuCl}_3 \cdot 3\text{H}_2\text{O}$  ( $5 \times 10^{-6}$  mol; 0.0013 g) and  $\text{FeCl}_3$  ( $5 \times 10^{-6}$  mol; 0.0008 g) were mixed with 0.0287 g of PVP ( $2.5 \times 10^{-4}$  mol) in 4.8 mL of glycol.<sup>25</sup> Then the mixture was treated as mentioned above, and PVP-stabilized nanoparticles were obtained after microwave irradiation for 30 s. When 0.0026 g of  $\text{H}_2\text{PtCl}_6 \cdot 6\text{H}_2\text{O}$  ( $5 \times 10^{-6}$  mol) and 0.0008 g of  $\text{FeCl}_3$  ( $5 \times 10^{-6}$  mol) were used, similar black PVP-stabilized nanoparticles were also obtained. Because the molar ratios between initial iron ions and ruthenium ions or platinum ions were both 1:1, we called these two colloids Fe/Ru (at 1:1) and Fe/Pt (at 1:1) alloys, respectively. When the initial  $\text{FeCl}_3$  was increased to 0.004 g ( $2.5 \times 10^{-5}$  mol) with amounts of  $\text{RuCl}_3 \cdot 3\text{H}_2\text{O}$  or  $\text{H}_2\text{PtCl}_6 \cdot 6\text{H}_2\text{O}$  and PVP fixed, the colloids obtained were called Fe/Ru (at 5:1) or Fe/Pt (at 5:1).

During catalyst purification, acetone is normally added to the colloid to precipitate nanoparticles, leaving contaminating ions such as chlorine ions in the supernatant. Glycol or methanol is then normally used to disperse the precipitate. However, in the present experiment, to eliminate chlorine ions, we substituted ammonia for NaOH<sup>22–24</sup> to produce  $\text{NH}_4\text{Cl}$ . Because  $\text{NH}_4\text{Cl}$  decomposes at high temperatures, it is easy to remove during the nanoparticle annealing process.

**SWNTs Growth.** Substrates used in this experiment are all  $\text{SiO}_2$  (400 nm)-coated silicon substrates prepared by thermal oxidation. Before use, the substrates were cleaned with acetone, methanol, deionized water and dried under a stream of dry  $\text{N}_2$ . The nanoparticle colloid was then spin-coated onto the substrate at a rate of 3500 rpm. An alternative way of coating the substrates was first to treat the substrates with piranha ( $\text{H}_2\text{SO}_4/\text{H}_2\text{O}_2$ , 7:3) and then after washing with deionized water to incubate them in the nanoparticle colloid for 10–30 min. Adsorption of nanoparticles on substrates could be fulfilled because of the H-bond interaction of exposed oxygen of PVP and Si–OH. The substrates with nanoparticles were then annealed in air at 600 °C for 30 min to remove the PVP organic layers and the  $\text{NH}_4\text{Cl}$ .

Subsequent growth of SWNTs was carried out in a quartz tube (~4 cm diameter) heated by a programmable horizontal furnace. MgO-supported iron oxide catalyst<sup>26</sup> powder was placed in front of the silica substrate to act as a “promoter”.<sup>27</sup> The furnace temperature was ramped up to 900 °C at a flow rate of 300 sccm argon (99.1%), and methane (99.9%) was then added at a flow rate of 200 sccm for a further 30 min. The system was then allowed to cool to room temperature under argon at a flow rate of 300 sccm.

Obviously, the substrates are very clean without amorphous carbon deposits owing to little self-pyrolysis of methane. It is noteworthy that when carrying out a comparative experiment without the promoter, a ceramic boat used for holding substrates turned a bit black and amorphous carbon deposits formed on the substrate. Clearly, the role of promoter is significant in preventing the self-pyrolysis of methane. It was regarded that catalytic pyrolysis of methane on the “promoter” generated hydrogen and benzene molecular. Then, hydrogen slows down methane decomposition on the silicon substrate and the active benzene molecular promotes the surface growth.<sup>27</sup>

**Characterization.** High-resolution transmission electron microscopy (HRTEM) and energy-dispersive X-ray analysis (EDAX) were used to investigate the structure and composition of nanoparticles. HRTEM images and EDAX spectra were collected using an FEI Tecnai F30 FEG operated at 300 kV. The diameters of nanoparticles and carbon nanotubes were determined by atomic force microscopy (Digital Instrument, Nanoscope III) using tapping mode. A Renishaw 1000 micro-Raman system (He–Ne laser excitation wavelength of 632.8 nm, spot size ~1  $\mu\text{m}$  diameter) was used to characterize SWNTs. For Raman study, the sample was placed directly on the test floor without any further treatment.

### Results and Discussion

**Characterization of Catalysts.** Figure 1 shows typical AFM images of Fe, Ru, Pt, Fe/Ru (at 1:1), and Fe/Pt (at 1:1) nanoparticles after annealing at 600 °C. Corresponding histograms of nanoparticles size are also shown. The diameters of Fe, Ru, and Fe/Ru (at 1:1) nanoparticles were distributed in the range of 0.5–2.3 nm, 0.7–2.9 nm, and 0.5–2.7 nm, respectively. In the case of nanoparticles containing Pt, both single Pt nanoparticles and Fe/Pt alloys seemed to aggregate slightly after annealing at 600 °C. Pt nanoparticles were distributed in a wider range, 0.7–4.5 nm, after annealing than before annealing (0.6–3 nm). For Fe/Pt (at 1:1) alloys, except for a few very large nanoparticles, ~13 nm located on the surface, most were quite uniform with a narrow size range of 0.5–2.7 nm. The large particles possibly formed by aggregation of mobile nanoparticles not firmly attached to the silica substrate. These were ignored when calculating the average nanoparticle size. From measurement of more than 120 nanoparticles,

(22) Yan, X. P.; Liu, H. F.; Liew, K. Y. *J. Mater. Chem.* **2001**, *11*, 3387.

(23) Tu, W. X.; Liu, H. F. *J. Mater. Chem.* **2002**, *10*, 2207.

(24) Yu, W. Y.; Tu, W. X.; Liu, H. F. *Langmuir* **1999**, *15*, 6.

(25) Dickey, E. C.; Grimes, C. A.; Jain, M. K. *Appl. Phys. Lett.* **2001**, *79*, 4022.

(26) Li, Q. W.; Yan, H.; Zhang, J.; Liu, Z. F. *J. Mater. Chem.* **2002**, *12*, 1179.

(27) Franklin, N. R.; Dai, H. J. et al. *Adv. Mater.* **2002**, *12*, 890.

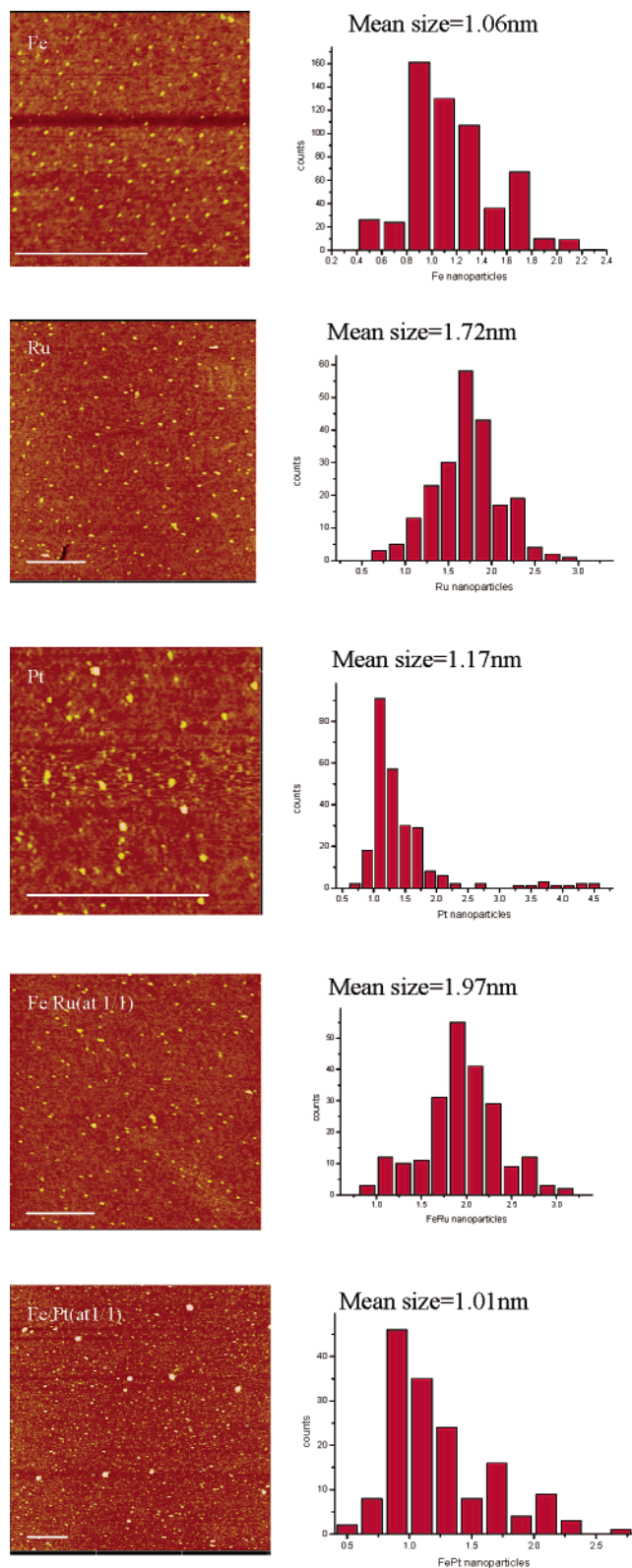


**Figure 1.** AFM images of Fe, Ru, Pt, Fe/Ru (1:1), and Fe/Pt (1:1) nanoparticles and their corresponding diameters distribution in turn (the scale bar equals 1  $\mu\text{m}$  and the height data scale is 8 nm).

mean sizes of Fe, Ru, Pt, Fe/Ru (at 1:1), and Fe/Pt (at 1:1) were 1.06, 1.72, 1.17, 1.97, and 1.01 nm, respectively.

To obtain some idea of the structure and composition of Fe/Ru (at 1:1) and Fe/Pt (at 1:1) nanoparticles, using

HRTEM and EDAX, it was necessary to analyze the nanoparticles before annealing. Figure 2a and b show TEM images of Fe/Ru (1:1) and Fe/Pt (at 1:1) nanoparticles. Sizes were similar to the AFM results above. Judging from the lattice fringes, most of the nanoparticles appeared to be single crystals. EDAX results showed that Fe/Ru (1:1) nanoparticles had the composition of iron and ruthenium in the molar ratio of 1.29, close to the initial molar ratio in the preparation process. For Fe/Pt (1:1), EDAX spectrum showed that nanoparticles contained iron and platinum. With our current software, it was not possible to obtain the iron/platinum molar ratio.

The formation of bimetallic nanoparticles is possibly due to a strong protective ability of PVP on both Fe and Ru or Fe and Pt monometallic clusters. In the preparation of bimetallic catalysts, both iron and ruthenium ions or both iron ions and  $[\text{PtCl}_6]^{2-}$  complex ions could be attached to the C=O group or N atom of PVP. The glycol reduction of these ions then resulted in the formation of bimetallic nanoparticles, which were stabilized by PVP.

We have also investigated the effect of higher Fe/Ru ratios on nanoparticles. When the initial ratio of Fe/Ru was increased from 1:1 to 10:1, it was obvious that results were extremely variable and some very large nanoparticles formed,  $\sim > 10$  nm (Figure 2c). Whereas nanoparticles in the diameter of  $\sim 2$  nm were single crystals, some nanoparticles larger than 5 nm displayed a polycrystalline structure (Figure 2c). EDAX results showed a higher molar ratio of Fe/Ru 5.1:1, compared with 1.29:1 for Fe/Ru (1:1) nanoparticles. The reason for the formation of polycrystalline structures is not known but could be due to the formation of single crystalline iron grains mixed with the alloy and resulting from the high iron content. We have tested other different molar ratios between  $\text{FeCl}_3$  and  $\text{RuCl}_3 \cdot 3\text{H}_2\text{O}$  such as 2 and 5, and ultimately the proper molar ratio for the formation of uniform and small Fe/Ru alloys is found to be 1/1–2/1.

**Growth and Characterization of SWNTs using Bimetallic Catalysts.** Figure 3 shows the highly efficient growth of SWNTs on surfaces using Fe/Ru (1:1) and Fe/Pt (1:1) catalysts. The growth conditions were described above. In terms of the ratio of the number of SWNTs grown to the number of the total nanoparticles employed, the growth efficiency is about 36% for Fe/Ru (1:1) and about 30% for Fe/Pt (1:1) (more than 1000 nanoparticles counted).

Most of the carbon nanotubes grown from Fe/Ru (1:1) appeared to be straight and short in length, 0.15–5  $\mu\text{m}$ . In contrast, nanotubes derived from Fe/Pt (1:1) were mostly curved and were mainly several micrometers long. The curvature of nanotubes grown from Fe/Pt (1:1) nanoparticles may be attributed to flexibility due to relatively high aspect ratios.<sup>10</sup> The diameters of nanotubes grown from both Fe/Ru (1:1) and Fe/Pt (1:1) were distributed mainly in the range 1–2.5 nm, with peak diameters of 1.74 and 1.06 nm, respectively (about 400 carbon nanotubes measured). Furthermore, diameters of carbon nanotubes were clearly close to the sizes of Fe/Ru (1:1) and Fe/Pt (1:1) nanoparticles before CVD growth, suggesting that the growth of SWNTs followed a VLS mechanism. This is supported by the fact that

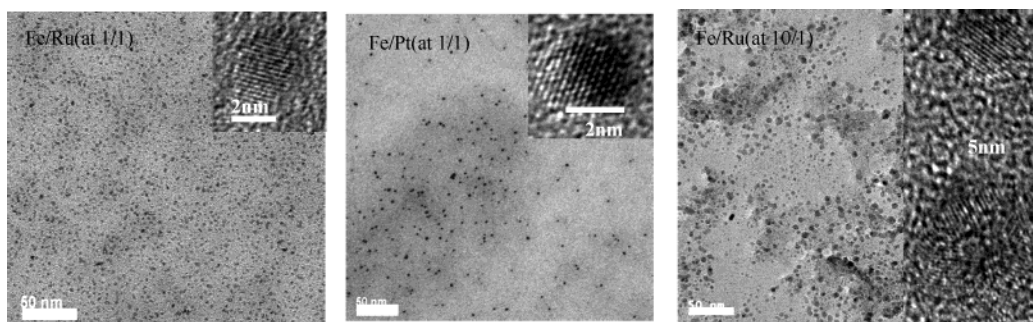


**Figure 2.** TEM and HRTEM images of Fe/Ru (1:1), Fe/Pt (1:1), and Fe/Ru (10:1) nanoparticles, left to right.

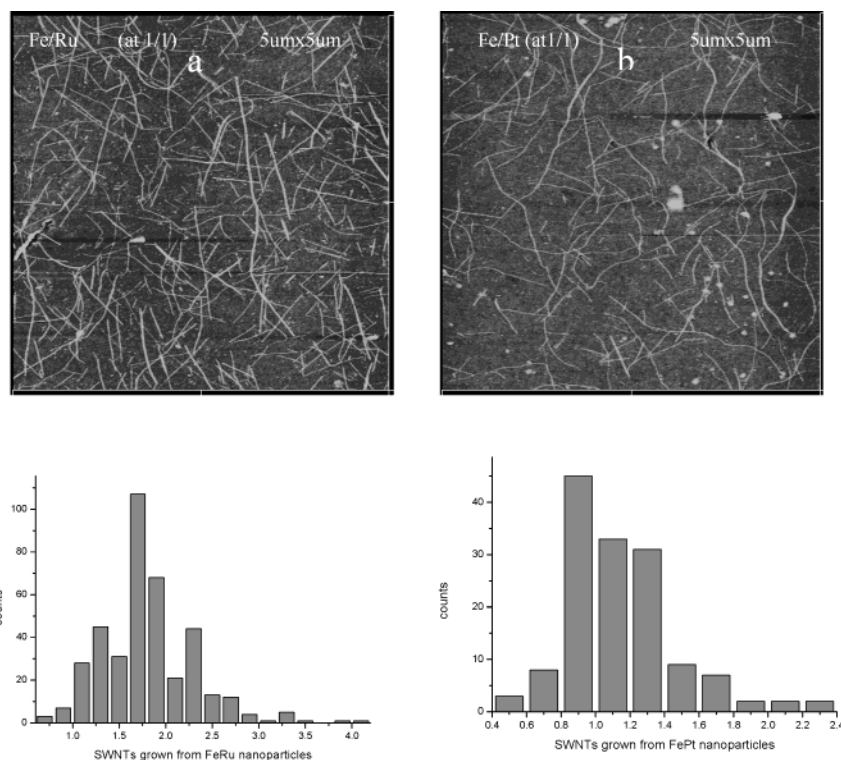


**Figure 3.** AFM images (height data scale = 5 nm) of SWNTs grown from Fe/Ru (1:1) (a) and Fe/Pt (1:1) (b). Below a and b are their corresponding diameter distributions.

some AFM images clearly display nanoparticles attached at one end of nanotubes (Figure 6f).

Raman spectroscopy has been shown to be a powerful tool in characterizing SWNTs, in which four Raman bands are strongly resonance enhanced. Three of them are located around  $1600\text{ cm}^{-1}$ , corresponding to the characteristic  $A_{1g}$ ,  $E_{1g}$ , and  $E_{2g}$  modes of the graphene sheet. The fourth strong band appears around  $200\text{ cm}^{-1}$  and it is unique to SWNTs arising from the radial breathing mode (RBM). Figure 4a and b are typical Raman spectra corresponding to carbon nanotubes grown from Fe/Ru (1:1) and Fe/Pt (1:1) nanoparticles. Typical SWNTs axial vibration modes around  $1590\text{ cm}^{-1}$  and RBM around  $105\text{--}195\text{ cm}^{-1}$  confirm the high quality of SWNTs on these substrates.

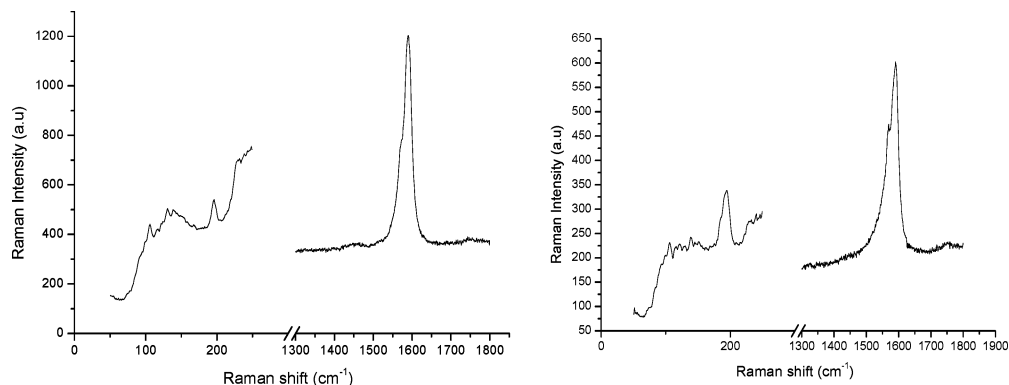
The Raman shift of the RBM ( $\omega_{\text{RBM}}$ ,  $\text{cm}^{-1}$ ) for an individual SWNT is related to its diameter ( $d$ , nm) by  $d = 248\text{ cm}^{-1}\text{ nm}/\omega_{\text{RBM}}$ .<sup>33</sup> Therefore, the four peaks of nanotubes grown from Fe/Ru (1:1) at  $106.1$ ,  $130.6$ ,  $139.6$ , and  $196.1\text{ cm}^{-1}$  correspond to SWNT diameters of  $2.34$ ,  $1.90$ ,  $1.78$ , and  $1.26\text{ nm}$ , respectively. The calculated mean diameter was  $1.82\text{ nm}$ , which is close to the size obtained from AFM topographic height images. SWNTs

grown from Fe/Pt (1:1) usually produced only one strong peak at around  $195.0\text{ cm}^{-1}$ . This corresponded to a SWNT diameter of about  $1.27\text{ nm}$ , which was not in good agreement with AFM topographic height data. We think that the existence of some weak peaks and the strong background peak of silicon substrate at  $300\text{ cm}^{-1}$  affected the consistence of these two results. As mentioned in the Experimental Section, samples for Raman test were directly investigated without making use of surface-enhanced Raman effect.<sup>10,28</sup> Furthermore, we affirm that Raman signals of SWNTs could be detected almost everywhere that we focused the laser spot, further proving the high density of SWNTs on the substrates.

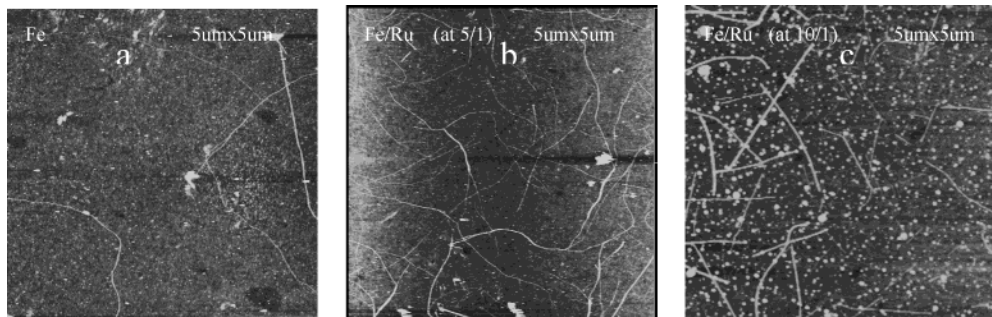
#### Effect of Catalyst Components on SWNT Growth.

Figure 5a shows one typical AFM image of SWNTs grown from either iron or ruthenium catalysts under the same condition as bimetallic catalysts. Obviously, only sparse SWNTs could be obtained, compared with SWNTs grown from bimetallic catalysts. When Pt

(28) Corio, P.; Brown, S. D. M.; Marucci, A.; Pimenta, M. A.; Kneipp, K.; Dresselhaus, G.; Dresselhaus, M. S. *Phys. Rev. B* **2002**, *61*, 13202.



**Figure 4.** Raman spectra of SWNTs grown from Fe/Ru (1:1) (left) and Fe/Pt (1:1) (right).



**Figure 5.** AFM images of SWNTs grown from Fe (a), Fe/Ru (5:1) (b), and Fe/Pt (10:1) (c).

nanoparticles were used, SWNTs could be barely observed on surfaces (data not shown), implying that Pt nanoparticles seemed to have no catalytic activity for nanotube growth.

When the initial ratio of Fe/Ru or Fe/Pt was increased from 1:1 to 5:1 and then to 10:1, the growth efficiency gradually reduced. The highest yields of SWNTs were obtained by using both Fe/Ru (1:1) and Fe/Pt (1:1). Figure 5b and c show the SWNTs growth using Fe/Ru (5:1) and Fe/Ru (10:1). The diameters of nanotubes grown from Fe/Ru (5:1) and Fe/Ru (10:1) were distributed mainly in the range of 0.5–2.3 nm and 0.7–2.9 nm, with peak diameters of 1.06 and 1.12 nm, respectively. Obviously, the diameters of SWNTs grown from both Fe/Ru (5:1) and (10:1) were mainly smaller than 3 nm, indicating only small nanoparticles were active for SWNTs growth. It was discussed above that some large Fe/Ru nanoparticles formed when the initial ratio of Fe/Ru was increased from 1:1 to 10:1 (Figure 2c). Therefore, one possible explanation for the relatively low efficient SWNT growth using both Fe/Ru (5:1) and Fe/Ru (10:1) is that some nanoparticles are too large to nucleate the growth of SWNTs.

**Effect of Methane Flow on SWNT Growth.** Figure 6 shows the growth of SWNTs on surfaces at different flow rates of methane. Figure 6a and b show the SWNTs growth using Fe/Ru (1:1) at a low flow rate of methane (50 sccm) and a high flow rate of methane (500 sccm), respectively. Clearly, more SWNTs were yielded on surfaces at a flow rate of 500 sccm methane than at a flow rate of 50 sccm methane. However, both low (50 sccm) and high (500 sccm) flow rates of methane yielded less SWNTs on surfaces than a flow rate of 200 sccm methane. As shown in Figure 6a, most SWNTs grown under a flow rate of 50 sccm methane were thinner than 2 nm and shorter than 5  $\mu\text{m}$ . In contrast, the diameters and the lengths of SWNTs grown under a flow rate of

500 sccm methane were distributed mostly in a wide range of 1–7.7 nm and hundreds of nanometers to tens of micrometers, respectively. This may imply that a high flow rate of carbon source could lengthen carbon nanotubes and enlarge the diameters of nanotubes when Fe/Ru (1:1) nanoparticles were used.

Figure 6c and d show the SWNTs using Fe/Pt (1:1) nanoparticles at flow rates of 50 and 500 sccm methane, respectively. Surprisingly, more SWNTs were yielded at a low flow rate of 50 sccm methane than at a high flow rate of 500 sccm. In addition, the diameters of SWNTs grown at flow rates of 50 and 500 sccm methane were both smaller than 3 nm. Particularly, because of many extremely thin SWNTs ( $\leq 1$  nm) formed at a flow rate of 500 sccm methane, a 1.5  $\mu\text{m}^2$  region instead of a 5  $\mu\text{m}^2$  region was used to display the SWNTs clearly.

The above results revealed the different catalytic behaviors between Fe/Ru (1:1) and Fe/Pt (1:1) nanoparticles at a low and a high flow rate of methane. We speculated that the different sizes of Fe/Ru (1:1) and Fe/Pt (1:1) nanoparticles might have an effect on the catalytic behavior. As shown in Figure 1, the mean size of Fe/Ru (1:1) nanoparticles was larger than that of Fe/Pt (1:1) nanoparticles. Therefore, assuming that dissolved carbon atoms first diffuse through the nanoparticles and then could reach the nucleation sites, a long diffusion distance resulted from the large size of Fe/Ru (1:1) nanoparticles. At a low flow rate of methane using Fe/Ru (1:1) nanoparticles, the dissolved carbon atoms capable of reaching nucleation sites were insufficient due to the long diffusion distance and hence the nucleation was not much. When the flow rate of methane was increased, the nucleation was thus enhanced. For Fe/Pt (1:1) nanoparticles in relatively small size, the nucleation would be possibly easy to achieve even at a low flow rate of methane. However, when the flow rate of methane was too high, rapid diffusion and

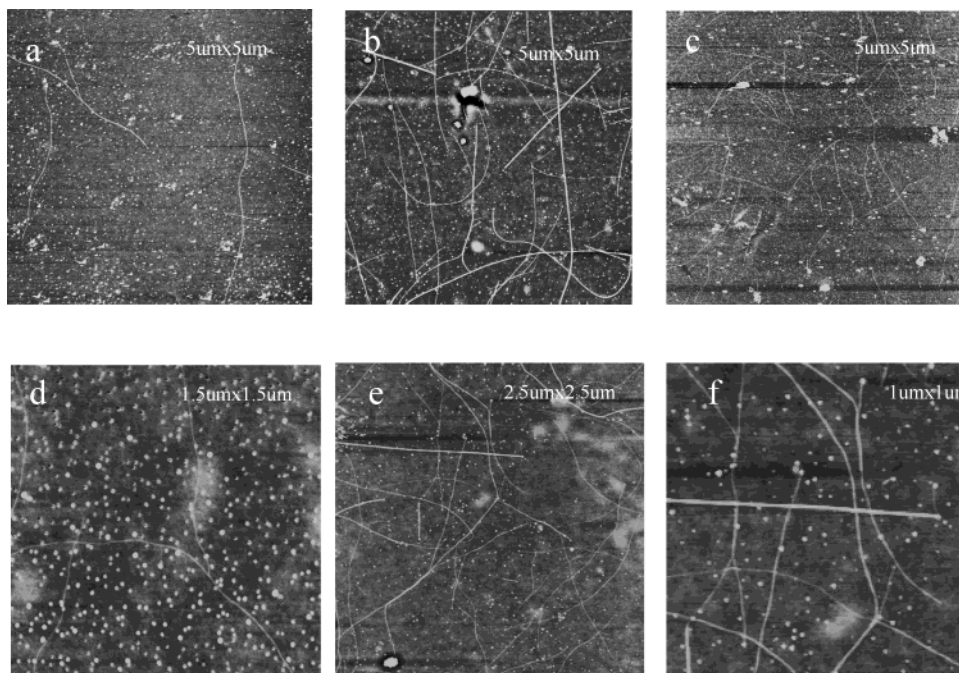


**Figure 6.** AFM images of SWNTs grown from Fe/Ru (1:1) at flow rates of 50 sccm methane (a) and 500 sccm methane (b), Fe/Pt (1:1) at flow rates of 50 sccm methane (c) and 500 sccm methane (d), and Ru at a flow rate of 500 sccm methane (e). (f) is the high-magnification image of (e). The height data scale for all is 5 nm.

precipitation of carbon may cause the formation of a carbon shell around nanoparticles rather than one-dimensional carbon nanotubes.

In the case of single-component catalysts such as iron and ruthenium, SWNTs grown under a flow rate of 50 sccm methane could be barely observed on surfaces (data not shown). Figure 6e shows SWNTs grown from Ru at a flow rate of 500 sccm methane, with a much higher yield of SWNTs than SWNTs grown at a flow rate of 200 sccm methane. Similar results were obtained when iron nanoparticles were used. Noteworthy was that in many previous studies,<sup>11,12,14,16</sup> surface growth of SWNTs using iron catalysts was carried out at a high flow rate of 800–1000 sccm methane. This might indicate that using iron or ruthenium nanoparticles, a high flow rate of methane increased the carbon diffusion rate and thus favored the growth of SWNTs on surfaces. Whereas for Pt nanoparticles, still no SWNTs were obtained under either low or high flow rates of methane, showing its inactivity toward catalytic growth of carbon nanotubes.

**Reasons for the High Efficiency of Bimetallic Catalysts.** There exists a lot of research based on classical, semiempirical, and quantum molecular dynamics simulations to illustrate the growth mechanisms for SWNTs. The prevailing view is that the SWNT growth via CVD follows the VLS model.<sup>29</sup> First, decomposed carbon atoms dissolve into nanoparticles and form a solid-state solution. Once the solution reaches its supersaturating point, carbon atoms precipitate from the alloy in the form of tubular structures. In a whole process, nucleation is regarded as a crucial stage. One of the models proposed that temperature and concentration gradients are main driving forces for carbon diffusion and precipitation<sup>30,31</sup> during nucleation. Because hydrocarbon molecules are exothermally decomposed on

the exposed surfaces of the nanoparticle, a temperature and a concentration gradient may form due to overheating and carbon dissolution of the surface part. The dissolved carbon atoms then precipitate on the cool surface of the nanoparticle because of the relatively low dissolvability of the cool part. The precipitated carbon atoms then assemble in the form of a graphitic layer. In this process, the wetting ability of a metal droplet on substrates plays a key role in the initiation of a graphene formation. For example, if a droplet loses contact with substrates, hydrocarbon molecules can impinge on the surface of the nanoparticle in all directions, leaving no cool surface to nucleate the SWNT growth.

A nucleation stage of SWNTs also involves bending of graphitic sheets in the form of graphene caps. The formation of a graphene cap on the particle surface is favored by diminishing total surface energy, avoiding energetically unfavored dangling bonds of open graphene edges.<sup>32</sup> Bending of a graphitic sheet occurs through overlapping the orbital of metal with the unsaturated  $sp^2$  orbital of the border of a graphene sheet. So, the electronic orbital property of nanoparticles may be important for the formation of graphene caps.

In conclusion, three factors of nanoparticles may be crucial in a SWNT growth process. First of all, the ability of nanoparticles in catalytically dehydrogenating the hydrocarbon molecular and in dissolving carbon atoms is important for the initiation of nucleation. Second, the wetting ability of nanoparticle droplets on substrates plays a key role in the nucleation. Third, the

(30) Baker, R. T. K.; Barder, M. A.; Waite, R. J. et al. *J. Catal* 1972, 26, 51.

(31) Kanzow, H.; Adalbert, D. *Phys. Rev B* 1999, 60, 11180.

(32) Dai, H. J.; Rinzler, A. G.; Smalley, R. E. et al. *Chem. Phys. Lett.* 1996, 260, 471.

(33) Jorio, A.; Saito, R.; Lieber, C. M.; McClure, T.; Dresselhaus, G.; Dresselhaus, M. S. et al. *Phys. Rev. Lett.* 2001, 86, 1118.

(29) Wagner, R. S.; Ellis, W. C. *Appl. Phys. Lett.* 1964, 4, 8.

electronic orbital property of nanoparticles may have an effect on the formation of graphene caps.

Fe, Ru, and Pt nanoparticles have been reported to be active toward the decomposition of methane and capable of dissolving carbon atoms. However, for Pt nanoparticles, judged from the phase diagram of Pt and C, a temperature higher than 1500 °C is probably required to precipitate carbon from the Pt–C alloy. Thus, under our reaction temperature of 900 °C, single Pt nanoparticles incapable of precipitating carbon atoms showed no activity toward the SWNT growth.

Possible reasons for the synergistic effect of Ru or Pt when alloyed with iron may be elicited from three aspects: first, the enhanced ability of bimetallic nanoparticles in decomposing methane and in dissolving carbon atoms; second, the improved wetting ability of bimetallic nanoparticles on SiO<sub>2</sub> surface; third, the stronger binding energy between bimetallic nanoparticles and graphene sheets for the formation of graphene caps. More work is needed to further understand the high activity of bimetallic nanoparticles.

### Conclusion

The main results presented in this study are summarized as follows. (1) We have modified the method of producing noble metal nanoparticles through chemical reduction associated with microwave irradiation<sup>22–24</sup> to obtain bimetallic nanoparticles such as Fe/Ru (1:1) and Fe/Pt (1:1) alloys in a narrow size distribution of 0.5–3 nm. High-resolution transmission electron microscopy

(HRTEM) and energy-dispersive X-ray analysis (EDAX) show that these nanoparticles are highly crystalline structures containing Fe and Ru or Fe and Pt. (2) Compared with single-metal Fe, Ru, and Pt nanoparticles of similar size, the use of bimetallic catalysts Fe/Pt and Fe/Ru improved the production of SWNTs on surfaces by at least 200%. Characterization of AFM confirmed that SWNTs grown from bimetallic catalysts were in high density on surfaces. (3) Initial ratios of Fe/Ru or Fe/Pt and the growth condition such as a flow rate of methane were found to be crucial for achieving high growth efficiency. (4) Possible reasons for the high efficiency of bimetallic nanoparticles were discussed. We speculate that the synergistic effect of bimetallic nanoparticles may result from their enhanced ability in decomposing methane and in dissolving carbon atoms, their improved wetting ability of bimetallic nanoparticles on SiO<sub>2</sub> surfaces, and the strong binding energy between bimetallic nanoparticles and graphene sheets. Further study of the bimetallic nanoparticles to fully understand their catalytic activity is still underway.

**Acknowledgment.** We are grateful for the financial support from National Natural Science Foundation of China (NSFC 90206023) and Ministry of Science and Technology of China (2001CB6105). We are also grateful to Prof. C. Robinson (University of LEEDS) for his kind help and useful discussion.

CM035070U